

## Research Paper

# An Experimental Study on the Thermal Efficiency of a Passive Solar Air Collector

Jacek Jan FIUK, Krzysztof DUTKOWSKI, Piotr PIĄTKOWSKI

*Faculty of Mechanical Engineering  
Koszalin University of Technology*

Raławicka 15/17, 75-453 Koszalin, Poland  
e-mail: jacek.fiuk@tu.koszalin.pl

This paper presents the results of an experimental investigation on a prototype flat passive solar air collector. The collector consists of an aluminum casing, transparent cover, air inlet and outlet channels and a flat absorber plate mounted inside the casing. The design is unique because the cover is made of transparent cellular polycarbonate sheet, a material whose application to passive solar collectors has not been extensively researched. The cover is 5 mm thick. The airflow through the collector is driven by natural convection. The study was performed on a laboratory set-up consisting of vertically mounted collector, external source of thermal radiation in the form of infrared lamps, measurement equipment and data acquisition system. The tests were performed for a range of irradiance  $G = 0\text{--}540\text{ W/m}^2$ . The following parameters were determined: absorber surface temperature, air temperature increase  $\Delta T$ , collector heat output and efficiency. Comparing the obtained results to the available data on conventional glass-covered designs has shown that the optical performance of polycarbonate cover is lower. However, in terms of thermal efficiency this is compensated by good insulation. The measurements for the maximum attainable irradiance of  $G_{\max} = 540\text{ W/m}^2$  are as follows: the mean air velocity at inlet  $w = 1.1\text{ m/s}$ , the volumetric flow rate of air  $\dot{V} = 30\text{ m}^3/\text{h}$ , and the corresponding heat output and thermal efficiency  $Q = 386\text{ W}$  and  $\eta = 36\%$ , respectively.

**Key words:** passive solar air collector, experimental investigations, natural convection, thermal efficiency.

## NOTATIONS

- $A$  – absorber area [ $\text{m}^2$ ],
- $B$  – collector gap width [m],
- $c_p$  – specific heat at constant pressure [ $\text{J}\cdot\text{kg}^{-1}\cdot\text{K}^{-1}$ ],
- $d$  – diameter [m],
- $F_R$  – heat removal factor [–],
- $\dot{m}$  – mass flow rate [ $\text{kg}\cdot\text{s}^{-1}$ ],
- $H$  – height [m],
- $G$  – irradiance [ $\text{W}\cdot\text{m}^{-2}$ ],
- $L$  – length [m],

$Q$  – heat output [W],

$T$  – temperature [ $^{\circ}\text{C}$ ],

$T_G, T_L$  – characteristic temperatures of the collector [ $^{\circ}\text{C}$ ],

$U_L$  – overall heat loss coefficient of the collector [ $\text{W}\cdot\text{m}^{-2}\cdot\text{K}^{-1}$ ],

$\dot{V}$  – volumetric flow rate [ $\text{m}^3\cdot\text{s}^{-1}$ ],

$w$  – mean velocity [ $\text{m}\cdot\text{s}^{-1}$ ].

### Greek symbols

$\alpha$  – transmissivity of transparent cover [-],

$\tau$  – absorptivity of absorber surface [-],

$\omega$  – uncertainty of measurement or calculation,

$\rho$  – fluid density [ $\text{kg}\cdot\text{m}^{-3}$ ],

$\Delta T$  – air temperature difference [K],

$\eta$  – thermal efficiency [-].

### Subscripts

amb – ambient,

in – inlet,

out – outlet.

## 1. INTRODUCTION

The Sun is the primary source of all energy on Earth. Solar energy can be converted to various other forms of energy by different conversion mechanisms such as photothermal, photovoltaic and photobiochemical [1]. Photothermal conversion mechanisms may be classified as either passive or active. Passive methods do not require any additional power source (e.g., pumps, fans, etc.). Typical examples of passive processes include heating a building through the use of a properly constructed barrier (glass), drying of agricultural products, direct water heating through the walls of a storage tank, accumulation of the heat within building walls, and passive cooling using evaporation of water. Alternatively, an active photo-thermal energy conversion transforms solar energy into heat by using additional energy inputs for various system components (e.g., liquid solar collectors, solar ponds, solar chimneys, farms, solar power stations, heat pumps, etc.) [1].

Solar collectors may be divided into two categories in regard to the working fluid: liquid or air [2]. Solar air collectors can be used in drying applications for a variety of products, e.g., agricultural products, timber, biomass cultivation, waste biomass, building materials, etc. [3, 4]. It is also possible to use them for regulating the microclimate in agricultural products' storage facilities [5, 6], as well as for ventilating and heating enclosed industrial areas and storage. They can also be applied to passive solar chimneys [7–9], additional greenhouse heating [10, 11] and many other processes that require hot air [12, 13].

In the passive systems, the purchase and installation of the air collector is the only expense incurred by the investor, and there is no active power consumption which makes this technology even more attractive if the capital costs are not too high. Furthermore, air collectors provide additional financial benefits compared to liquid collectors that require additional costs associated with: implementation of an installation project, permit fees, construction, control system, a working fluid reservoir and the working fluid itself, intermediate heat exchangers, servicing, maintenance, etc.

When it comes to increasing the temperature of indoor air, passive solar air collectors are an excellent choice in places where windows cannot be considered due to either technical or safety issues. The common examples of such structures are heightened cellars, industrial areas, storage halls or workshops. There are however situations due to the building's orientation and localization when solar collectors cannot be mounted on certain walls (most commonly these are north-facing walls), as irradiation there is the lowest. Passive air collectors can be divided in regard to the source of the inlet air and the destination of the warmer outlet stream. In addition, passive solar air collectors can be used for both heating and cooling of the rooms [14]. Selected designs are described below.

In the first configuration (Fig. 1), the passive solar air collector can be used to heat a room next to a south-facing wall. The supply of cool air comes directly from the room itself, creating a recirculation pattern. This solution allows the fastest rate of temperature growth; however, its main flaw is the fact that only the quality of the air determined by smell or humidity can be considered as there is no fresh air being introduced into circulation.

The second configuration (Fig. 2) enables heating a room neighbouring the south side of a building with the air coming from either outside of the building or another room. This set-up allows for ventilating the space with fresh cool air that is being heated within the collector. The main difficulty of utilizing such

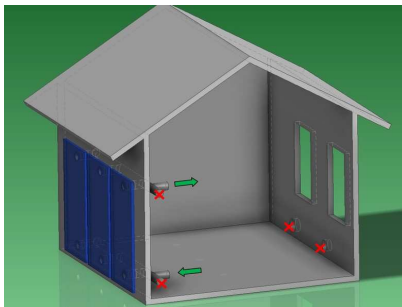


FIG. 1. Utilization of passive solar air collector to increase the temperature in a room bordering the south side of a building with air recirculation [14].

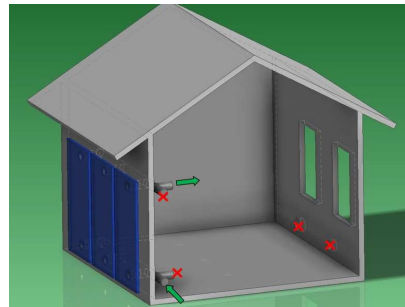


FIG. 2. Utilization of passive solar air collector to raise the temperature in a room bordering the side of a building side using an exterior air supply [14].

configuration is observed during colder seasons, such as winter or even autumn in certain regions of the world. During the cold season, the inlet air may have a temperature that is too low, and, as a result, a single collector may prove to be ineffective at providing the needed outlet temperature.

However, the solar air collectors have been of little interest to the investors in comparison to liquid collectors, and this is due to a lack of universal and reliable data on the effect of operating conditions on energy efficiency. Currently, tests of various prototypes of solar air collectors are being conducted in many countries.

ZHOU *et al.* [15] conducted a theoretical analysis along with numerical and experimental studies on the impact of solar chimney dimensions and irradiance  $G$  on the intensity of the ventilation process. In their study, the dimensions of the solar chimney, namely the height, width, and air gap thicknesses varied between 10–100 m, 0.5–5 m, and 0.1–2 m, respectively. Solar irradiance varied over the range of 400–1000 W/m<sup>2</sup>. The intensity of the ventilation process was characterized by the mass flow rate of air through the chimney. Studies have shown that there is an optimal air gap thickness corresponding to the thickness of the boundary layer at the outlet of the chimney. For devices with  $H = 10$ –30 m, the optimum thickness of the air gap was in the range of 0.2–0.4 m. The corresponding mass flow rate of air was approximately 0.4 kg/s.

ARCE *et al.* [16] studied a solar collector (solar chimney) with dimensions  $L \times H = 4.5 \times 1.0$  m and the air gap thickness of 0.3 m. Thermal and flow investigations were conducted under natural conditions. At the instance of maximum solar irradiance (604 W/m<sup>2</sup>), the increase in the temperature of the air flowing through the collector was 70°C and the convective air flow rate was 50–374 m<sup>3</sup>/h (corresponding to the average daily level of flow rate of 177 m<sup>3</sup>/h). Experimental studies have confirmed that the flow of air through the collector mainly depends on the temperature increase and the pressure changes caused by variations in the density of the air outside and inside the chimney.

CHEN *et al.* [17], using a laboratory solar chimney with electrically heated back wall, experimentally investigated the influence of geometrical parameters of a collector as well as the tilt angle and heat flux on the convective air mass flow. For a chimney with a constant height of 1.5 m and a width of 0.62 m, the maximum air flow was obtained when the thickness of the gap was 200 mm, and the collector was tilted from the vertical plane by 45°. The volume flow rate of air was 0.035 m<sup>3</sup>/s and was 45% higher than that obtained when the collector was in vertical position.

ALVAREZ *et al.* [18] presented the results of experimental investigations of a solar collector prototype that featured an absorber made of aluminium cans obtained from recycling. Sixteen parallel channels made of an arrangement of 128 black painted cans were placed under a glass cover. The study investigated

the experimental efficiency of the proposed collector. The results were compared with the results of other authors. In addition to the obvious advantages associated with using waste materials to build this prototype, an increase of more than 60% in the collector efficiency, relative to other designs incorporating absorber surface expansion was found.

The concept of using waste aluminum cans to build an air collector was also described in the works of OZGEN *et al.* [19, 20]. The authors experimentally determined the efficiency of three solar prototypes featuring dual-flow technology (with a flow above and below the absorber). For the experimental investigations, different arrangements were tested, namely the cans arranged in lines on both sides of the absorber and cans arranged in a zigzag pattern on both sides of the absorber. All the designs worked concurrently in natural sunlight and with forced air flow with mass flow rates of 0.03 kg/s or 0.05 kg/s. A greater efficiency was obtained for  $G = 0.05$  kg/s. The highest efficiency was obtained for the air collector with the cans arranged in a zigzag pattern. During the maximum solar radiation, the efficiency of the collector exceeded 70%.

There is a great need for experimental work since the amount of reliable data for passive solar air collector technology is relatively low, especially for passive collectors in a certain size group ( $\sim 1$  m width and  $\sim 2$  m height). The authors believe that the community including both the renewable energy technology providers and researchers would benefit greatly from such data. In addition, most existing publications show the results of the solar air collector investigations carried out under natural conditions, which are highly dependent on location, season, weather, and time of day, and because of this there may be substantial variation between operating conditions, i.e., irradiance, ambient temperature and air velocity in the local environment. This variation makes it difficult to conduct a comparison of the existing studies on solar air collectors.

This article aims to present the results of the experimental investigations of the prototype passive solar air collector with a flat absorber and cover made of transparent cellular polycarbonate sheet. The results of similar experimental investigations but with a collector covered with brown coloured polycarbonate sheet are presented in the work of DUTKOWSKI *et al.* [21]. The results obtained for flat absorber passive solar air collector will serve as a baseline for analysing further design refinements and alternatives.

## 2. EXPERIMENT

### 2.1. Solar air collector

Figure 3 shows an external view of the examined passive solar air collector prototype. The collector consists of an aluminium casing with the dimensions:

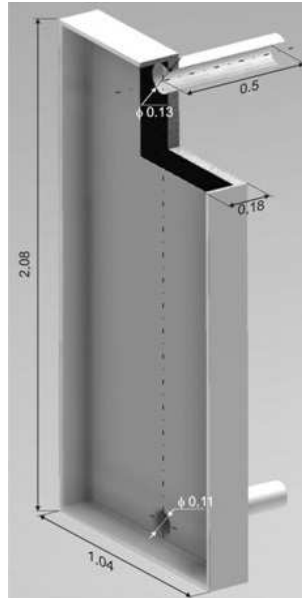


FIG. 3. View of tested solar collector.

1.04 m (width)  $\times$  2.08 m (height)  $\times$  0.18 m (depth). The back wall of the collector is insulated with mineral wool, 50 mm thick. The absorber is placed on the surface of the insulation and is made of a 0.5 mm thick aluminum plate coated with a thin layer of matte black paint. For temperature measurements, 12 K-type thermocouples were attached to the back surface of the absorber. The measured temperatures allowed to determine the time needed to achieve steady-state conditions as well as the temperature distribution on the absorber surface.

The side walls as well as the top and bottom surfaces are insulated with a 20 mm thick mineral wool. The transparent cover of the collector is made of a 5 mm thick transparent cellular polycarbonate sheet.

The air inlet to the collector is a circular duct with diameter  $d_{in} = 110$  mm and a length of 0.5 m. The air outlet duct has an internal diameter  $d_{out} = 130$  mm and a length of 0.5 m. The axes of inlet and outlet channels are located in the middle of collector widthwise, 90 mm from the lower edge of the collector and 110 mm from its upper edge.

### 2.2. Experimental set-up and procedure

A schematic of the experimental set-up is presented in Fig. 4. Its main part is the prototype solar air collector, which was mounted on the supporting struc-

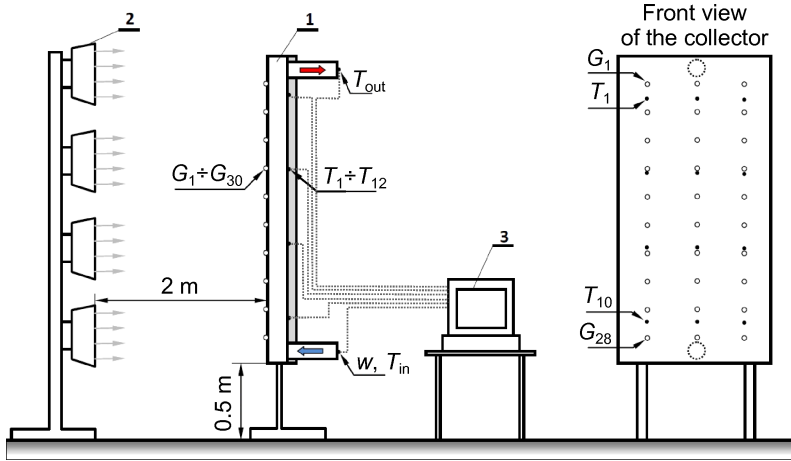


FIG. 4. Experimental set-up: 1 – air collector, 2 – adjustable radiation source, 3 – data acquisition system,  $T_1$ – $T_{12}$  – absorber surface temperature measurement locations,  $T_{in}$  – inlet air temperature,  $T_{out}$  – outlet air temperature,  $w$  – air velocity,  $G_1$ – $G_{30}$  – irradiance measurement locations.

ture. The collector was operated in a vertical position. The distance between the lower edge of the collector and the floor was 0.5 m.

The sources of radiation were infrared Philips HeLeN lamps. They were arranged equidistant from the collector front. The distance between the lamps and the transparent cover was 2 m. Total radiation reaching the collector surface was measured using a secondary standard pyranometer CMP11 by Kipp & Zonen. The value of the irradiance  $G$  was calculated by taking the arithmetic average of the 30 local values of irradiance, measured at uniformly distributed locations over the face of the collector (see Fig. 4 –  $G_1$ – $G_{30}$ ). The maximum value of the irradiance achievable under laboratory conditions was  $G = 540 \text{ W/m}^2$  and the uncertainty of irradiance measurement was  $\pm 4.33 \text{ W/m}^2$ .

Air temperature at the entrance of the inlet channel, air temperature at the end of the outlet channel, ambient temperature and temperature of the absorber surface (at 12 equally spaced points) were measured individually by K-type thermocouples. Every thermocouple was individually calibrated (over the range of  $20$ – $80^\circ\text{C}$ ) using a glass thermometer with a scale graduation of  $0.02^\circ\text{C}$  as the reference. The resulting uncertainty from calibration was at best  $\pm 0.2 \text{ K}$  for each thermocouple. All temperature signals were recorded every 20 s using a Memograph RSG40 Endress & Hauser recorder. Steady-state temperature measurements were taken as the average of readings recorded over a 5-minute period.

Air velocity at the collector inlet duct was measured by a thermo-anemometer (Testo 524). A weighted average of five measurements across the inlet (along the

vertical and horizontal axes) was used to determine the mean velocity. The uncertainty in a single velocity measurement was determined to be  $\pm 0.03 \text{ m/s} + 5\%$  of the measured value. Hence, the maximum error in velocity measurements was  $\pm 0.085 \text{ m/s}$ .

The temperature increase  $\Delta T$  of air flowing through the collector was determined as the difference between the temperature of air leaving the outlet channel  $T_{\text{out}}$  and the air temperature at the inlet to the collector  $T_{\text{in}}$ . It should be noted that the air temperature at the entrance of the collector is constant and corresponds to the ambient temperature  $T_{\text{amb}}$ , hence  $T_{\text{in}} = T_{\text{amb}} = 20^\circ\text{C} \pm 2^\circ\text{C}$ . Laboratory room was assumed to be a pseudo-infinite volume of air because of its dimensions ( $10 \times 16 \times 3 \text{ m}$ ) and the fact that it was open to adjacent rooms as well. The lack of significant influence of the output heat on ambient temperature was confirmed by the ambient temperature fluctuations not exceeding  $2^\circ\text{C}$ .

$$(2.1) \quad \Delta T = T_{\text{out}} - T_{\text{in}} = T_{\text{out}} - T_{\text{amb}}.$$

The volumetric flow rate of air through the collector was calculated from the values measured on the inlet channel using the following equation:

$$(2.2) \quad \dot{V} = w \cdot (0.25 \cdot \pi \cdot d_{\text{in}}^2),$$

where  $w$  is the mean air velocity at the inlet of the channel, and  $d_{\text{in}}$  is the diameter of the inlet channel. The heat output of the solar collector was determined according to the formula

$$(2.3) \quad Q = \dot{m} \cdot c_p \cdot \Delta T = \rho \cdot \dot{V} \cdot c_p \cdot \Delta T,$$

where  $\rho$  is the density of air (at the inlet), and  $c_p$  is the specific heat of air (at ambient temperature and constant pressure).

The thermal efficiency of the passive air collector is defined as

$$(2.4) \quad \eta = \frac{Q}{G \cdot A} = \frac{\rho \cdot \dot{V} \cdot c_p \cdot \Delta T}{G \cdot A},$$

where  $G$  is the average value of the irradiance reaching the front surface of the collector, and  $A$  is the absorber area.

### 2.3. Uncertainty analysis

The errors associated with the experimental measurements are presented in the paragraphs above, which describe the procedure. These errors result in the uncertainty of derived parameters such as thermal efficiency or heat output. However, the level of this uncertainty can be calculated using the Holman method. In general, the uncertainty of value  $X$  can be expressed as

$$(2.5) \quad \omega_X = \left[ \left( \frac{\partial X}{\partial y_1} \omega_{y1} \right)^2 + \left( \frac{\partial X}{\partial y_2} \omega_{y2} \right)^2 + \dots + \left( \frac{\partial X}{\partial y_n} \omega_{yn} \right)^2 \right]^{1/2},$$

where  $y_1, y_2, \dots, y_n$  are variables affecting the value of  $X$ , and  $\omega$  stands for uncertainty.

From Eqs. (2.4) and (2.5), the uncertainty of thermal efficiency  $\omega_\eta$  is given by:

$$(2.6) \quad \omega_\eta = \left[ \left( \frac{\dot{V} c_p \Delta T}{AG} \omega_\rho \right)^2 + \left( \frac{\rho c_p \Delta T}{AG} \omega_{\dot{V}} \right)^2 + \left( \frac{\rho \dot{V} \Delta T}{AG} \omega_{c_p} \right)^2 + \left( \frac{\rho \dot{V} c_p}{AG} \omega_{\Delta T} \right)^2 + \left( -\frac{\rho \dot{V} c_p \Delta T}{A^2 G} \omega_A \right)^2 + \left( -\frac{\rho \dot{V} c_p \Delta T}{AG^2} \omega_G \right)^2 \right]^{1/2}.$$

The uncertainty of heat output  $\omega_Q$  can be calculated in similar fashion. It is given by the following equation:

$$(2.7) \quad \omega_Q = \left[ \left( \dot{V} c_p \Delta T \omega_\rho \right)^2 + \left( \rho c_p \Delta T \omega_{\dot{V}} \right)^2 + \left( \rho \dot{V} \Delta T \omega_{c_p} \right)^2 + \left( \rho \dot{V} c_p \omega_{\Delta T} \right)^2 \right]^{1/2}.$$

In order to simplify this formula, the uncertainty of volumetric flow rate needs to be derived. The volumetric flow rate is calculated at the inlet channel using Eq. (2.2), therefore its uncertainty can be expressed as

$$(2.8) \quad \omega_V = \left[ \left( 0.25 \cdot \pi \cdot d_{in}^2 \cdot \omega_w \right)^2 + \left( 0.5 \cdot w \cdot \pi \cdot d_{in} \cdot \omega_d \right)^2 \right]^{1/2}.$$

A comprehensive summary of the presented uncertainty analysis is given in Table 1.

**Table 1.** Uncertainty in measurements and calculations.

No	Parameter	Instrument	Uncertainty $\omega$	Value
1	Air density	–	$\omega_\rho$	0*
2	Specific heat	–	$\omega_{c_p}$	0*
3	Temperature increase	K-Type thermocouple	$\omega_{\Delta T}$	$\pm 0.2$ K
4	Absorber dimensions	Tape ruler	$\omega_L, \omega_W$	$\pm 0.5$ mm
5	Absorber surface area	(calculated)	$\omega_A$	$\pm 1.1 \cdot 10^{-03}$ m <sup>2</sup>
6	Irradiance	Pyranometer CMP11 Kipp & Zonen	$\omega_G$	$\pm 4.33$ W/m <sup>2</sup>
7	Air velocity	Thermo-anemometer Testo 524	$\omega_w$	$\pm 0.085$ m/s
8	Inlet duct diameter	Tape ruler	$\omega_d$	$\pm 0.5$ mm
9	Max. volumetric flow rate	(calculated)	$\omega_V$	$\pm 2.87$ m <sup>3</sup> /h
10	Max. thermal efficiency	(calculated)	$\omega_\eta$	$\pm 3.4\%$
11	Max. heat output	(calculated)	$\omega_Q$	$\pm 36.8$ W

\* Values for density and specific heat taken from reference data [23].

### 3. EXPERIMENTAL RESULTS AND DISCUSSIONS

Experimental studies were carried out using the following procedure. After turning the measurement equipment on the value of electric current supplied to the radiation source was set using an autotransformer. In order to ensure the steady-state conditions, the experimental set-up was given time to reach equilibrium. A criterion for achieving steady-state conditions was a constant temperature at the absorber surface for a minimum of five minutes. Once the steady-state conditions were achieved, the local air velocity at the entrance to the inlet channel and the distribution of the irradiance on the front surface of the solar air collector were measured. Measurements of air velocity, irradiance, and the various temperatures were used to calculate the desired characteristic parameters, for example, the heat output of passive solar air collector.

In previous experimental studies by DUTKOWSKI *et al.* [21] the measurements of absorber temperature in a similar passive solar air collector were presented. In the case of currently examined prototype, the results are similar (not presented in this paper). These results show how the collector reached the steady-state working conditions. The main conclusion is that the steady-state is reached within approximately 15–20 min.

TANAKA *et al.* [22] as well as MANEewan *et al.* [12] arrived at similar values for their (similar) designs of solar air collectors to work in steady-state conditions. It is therefore safe to assume at this point that timescale for reaching the steady-state heat and fluid transfer is roughly 20 minutes.

#### 3.1. Air temperature increase

Figure 5 shows an increase of the air temperature  $\Delta T$  (Eq. (2.1)) through the collector as a function of irradiance  $G$ . It was found that the air temperature increased proportionally to the intensity of incident radiation.

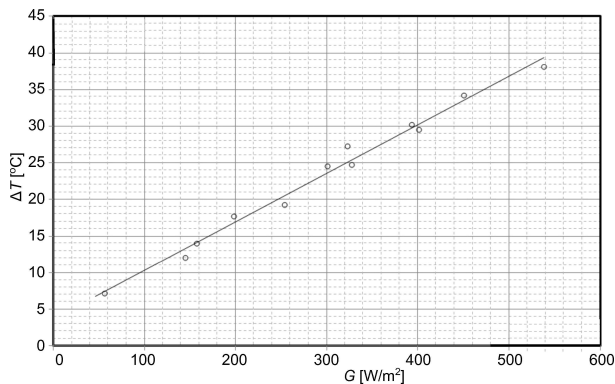


FIG. 5. Air temperature difference  $\Delta T$  vs. irradiation  $G$ .

The linear nature of the  $\Delta T$  change related to irradiance  $G$  is observed for both forced air flow through collector [24, 25] and during natural convection [13]. On the basis of experimentally confirmed correlations between an increase in air temperature and irradiance, it is recommended to use the equation [13]:

$$(3.1) \quad \Delta T = T_G \frac{G}{G_0} + T_L,$$

where  $G_0$  is the standard irradiance ( $1000 \text{ W/m}^2$ ) and  $T_G$  and  $T_L$  are the characteristic temperatures of the collector (see [13]). For the tested conditions, these values were  $T_G = 66^\circ\text{C}$  and  $T_L = 4^\circ\text{C}$ . According to Eq. (3.1), the theoretical temperature rise of the air flowing through the tested collector, at the standard irradiance  $G_0$ , is  $\Delta T(G_0) = 70^\circ\text{C}$ .

### 3.2. Velocity and volumetric flow rate

Average air flow velocity was measured for passive operating mode, that is, natural convection. Air is driven by the temperature gradient in the air gap between the collector cover and the absorber plate. Because of the constant (ambient) temperature of the air at the inlet duct entrance the air velocity measurement was taken there.

Figure 6 shows the results of the air velocity at the inlet channel entrance as a function of the irradiance. It was noted that when radiation increases, so does the average velocity of the flowing air. The maximum average velocity of the air flowing through the collector was approximately  $1.1 \text{ m/s}$ . The functional relationship between air velocity and irradiance was found to be logarithmic.

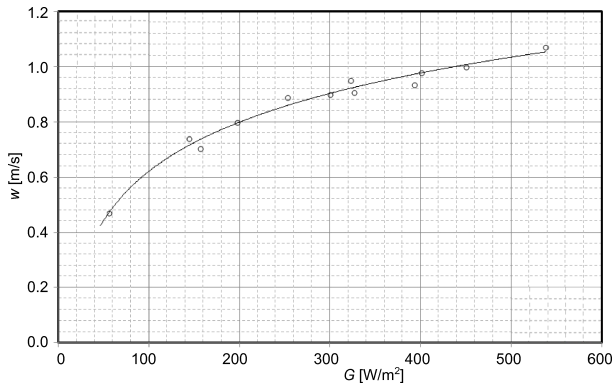


FIG. 6. Average air velocity  $w$  at the entrance to the inlet channel vs. irradiance  $G$ .

The volumetric flow rate of air was calculated using Eq. (2.2) and is dependent on the average flow velocity. As shown in Fig. 7, the maximum flow rate

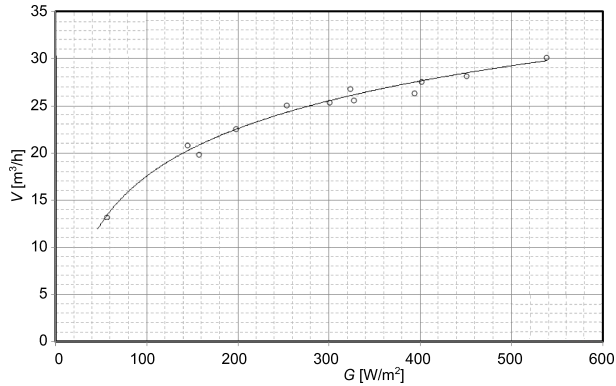


FIG. 7. Volumetric air flow rate  $\dot{V}$  vs. irradiance  $G$ .

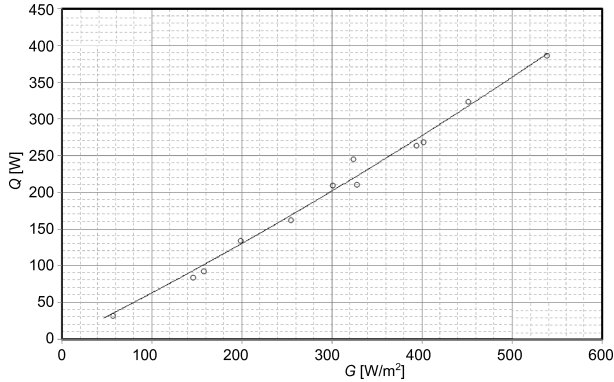
of air through the passive collector was  $\dot{V} = 30 \text{ m}^3/\text{h}$ . This value is almost ten times lower than that obtained at the corresponding irradiance ( $400 \text{ W}/\text{m}^2$ ) by RYAN & BUREK [26], who studied the convective air flow in a channel with a width of 1 m and at the air gap thicknesses of  $B = 0.02\text{--}0.15 \text{ m}$ . In the mentioned work, the inlet and outlet areas were much larger allowing for higher volumetric flow rate. The open inlet and outlet cross-section area was equal to the gap cross-section area. ZHAI *et al.* [27] studied natural convection induced air flow inside channels with an electrically heated back wall. In their study, the channel dimensions (width  $\times$  height  $\times$  air gap) were  $500 \times 1500 \times 200 \text{ mm}$ , and the channels were tilted at an angle of  $45^\circ$ . ZHAI *et al.* [27] used a heat flux of  $300 \text{ W}/\text{m}^2$  and an air volumetric flow rate of approximately  $80 \text{ m}^3/\text{h}$ , which is approximately three times higher than the result obtained in this paper. The authors [27] noted that operating at collector inclination angles other than  $45^\circ$  decreased the air flow rate. Lower air flow rates through collectors are caused by the negative interaction of inlet and outlet channel. The authors [27] reduced the cross-section area of air flow and additionally increased the pressure drop of air flow. In the previously mentioned articles, the inlet and outlet spaces of collector had no restrictions.

### 3.3. Heat output of the collector

Figure 8 shows the effect of irradiance  $G$  on the collector heat output  $Q$ , defined by the Eq. (2.3).

The increase of solar irradiance causes an increase in the heat output of the collector. The maximum heat output was approximately  $386 \text{ W}$  when the irradiance was  $540 \text{ W}/\text{m}^2$ .

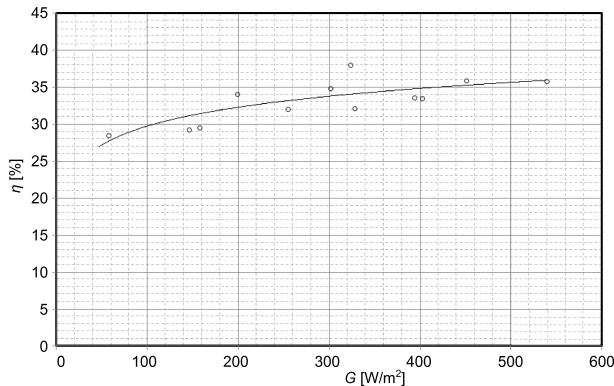
In a forced convection scenario, as described in the work of ZHAI *et al.* [27], it is shown that at a constant air flow rate, the relation between the heat output

FIG. 8. Collector heat output  $Q$  vs. irradiance  $G$ .

of solar air collector and irradiance is linear. In the case of natural convection, the constant air flow rate condition is no longer valid as the increase in irradiation creates larger temperature gradient which translates directly into density gradient – the driving force behind natural convection. In the examined prototype, this results directly in air flow velocity increase through the collector. The local cross-sectional area of the flow field is kept constant with time. This leads to a final conclusion that increasing the irradiance  $G$  causes the heat output to change in a non-linear fashion (see Eq. (2.4)). However, for a selected range of irradiance available in experimental set-up and current design constraints of prototype solar collector, the non-linear behaviour was not observed. This may indicate that the impact of increased mass flow rate is minor.

### 3.4. Thermal efficiency

Figure 9 shows the collector efficiency values for different values of the irradiance  $G$ .

FIG. 9. Influence of irradiance  $G$  on the thermal efficiency  $\eta$  of the collector.

Thermal efficiency of the solar air collector was calculated using Eq. (2.4). The results show that an increase in the irradiance increases the thermal efficiency of the collector. The maximum efficiency, obtained in this work, was approximately 38% for  $G = 323 \text{ W/m}^2$ . EL-SAWI *et al.* [28] obtained a thermal efficiency of  $\sim 35\%$  at  $G = 300 \text{ W/m}^2$  using a solar collector with a flat absorber operating under forced convection conditions ( $w = 0.040 \text{ kg/(m}^2\cdot\text{s)}$ ). The thermal efficiency of the collector, expressed as the ratio of useful heat supplied to the fluid and thermal power that reaches the collector through radiation, is defined by Eq. (2.4). The efficiency of a solar collector may also be determined using the Hottel-Whillier-Bliss equation [29]:

$$(3.2) \quad \eta = F_R \left[ (\tau\alpha) - U_L \frac{T_{\text{in}} - T_{\text{amb}}}{G} \right],$$

where  $F_R$  is the heat loss factor,  $\tau$  is the coefficient of heat transmission of the material covering the collector,  $\alpha$  is the absorption coefficient of the absorber surface, and  $U_L$  is the overall heat loss coefficient of collector [13]. Equation (3.2) is a linear function, which allows an easy determination of the efficiency of a collector, but it is only applicable for liquid collectors in the abovementioned form. In the case of passive air collectors, the inlet temperature of working fluid is the ambient temperature of air surrounding the collector,  $T_{\text{in}} = T_{\text{amb}}$ . Comparing Eqs. (2.4) and (3.2) allows for some modifications, so that the thermal efficiency of air collector can be represented as a linear function of the expression  $(T_{\text{out}} - T_{\text{amb}})/G$  [24, 30, 31]. In the modified form, applicable for air collector, it is written:

$$(3.3) \quad \eta = F_R \left[ (\tau\alpha) - U_L \frac{T_{\text{out}} - T_{\text{amb}}}{G} \right],$$

or

$$(3.4) \quad \eta = F_R (\tau\alpha) - F_R U_L \frac{T_{\text{out}} - T_{\text{amb}}}{G}.$$

In this equation, the parameters  $F_R(\tau\alpha)$  and  $F_R U_L$  describe the performance of the collector. Those are: representing the optical properties of the system term  $(\tau\alpha)$ , where  $\tau$  is the transmissivity of the transparent cover and  $\alpha$  is the absorptivity of the absorber surface, the overall heat loss coefficient of collector  $U_L$  and the heat removal factor  $F_R$ . Equation (3.4) indicates that a plot of instantaneous efficiency values against temperature rise factor  $(T_{\text{out}} - T_{\text{amb}})/G$  [32] will result in a straight line whose slope is equal to  $F_R U_L$  and the  $y$ -intercept is equal to  $F_R(\tau\alpha)$  (Fig. 10).

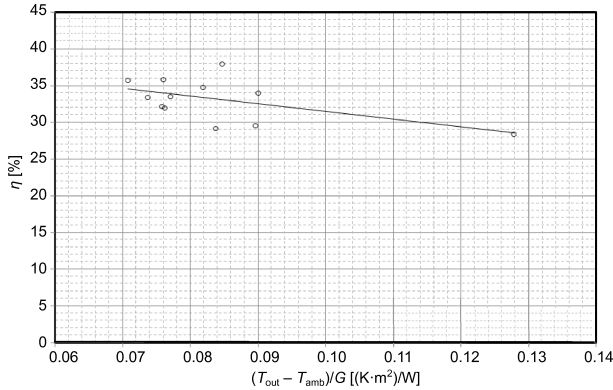


FIG. 10. Efficiency  $\eta$  of the solar air collector vs. the temperature rise factor  $(T_{out} - T_{amb})/G$ .

The respective efficiency equation and the values of  $F_R U_L$  and  $F_R(\tau\alpha)$  are

$$(3.5) \quad \eta = F_R(\tau\alpha) - F_R U_L \frac{T_{out} - T_{amb}}{G} = 0.42 - 1.05 \frac{T_{out} - T_{amb}}{G}.$$

It can be seen that the value of  $F_R U_L$  factor is very low. This can be due to a low value of the heat removal factor  $F_R$ . The low value of  $F_R U_L$  is caused by the relatively low heat losses through the collector casing and cover. This is caused by good thermal insulation and the absence of external factors intensifying heat transfer such as strong wind and low ambient temperature, and is shown in Fig. 10 as low slope of the linear characteristic, which also means that for a wide range of solar irradiance  $G$  the efficiency of the collector is kept at similar level.

The parameter  $F_R(\tau\alpha)$  accounting for the optical properties of the system, is equal to 0.42. This value is approximately 20% lower than the values presented in the literature for a glasscovered collector [30]. Preliminary research indicates that a cellular polycarbonate sheet has worse optical performance in relation to glass. However, this material is a preferred choice when weight and safety issues (non-shattering material) are important.

#### 4. SUMMARY AND CONCLUSIONS

The results of research on liquid operated solar collectors are frequently published in various journals. The analytical tools for assessing the thermal performance of such devices are well developed and proven. When it comes to solar air collectors, be it passive or active, the amount of publications is significantly smaller. This presents an opportunity to further develop this particular branch of solar energy devices and help with design refinement and performance optimization. There are many applications of passive solar air collectors.

In this paper, the results of an experimental investigation on flat passive solar air collector, covered with transparent cellular polycarbonate sheet have been presented. The collector worked under natural convection regime. The study was performed on a laboratory set-up and led to obtaining basic performance characteristics of this collector type. The measured parameters consisted of: collector irradiance, absorber surface temperature distribution, air temperature increase between inlet and outlet, and air velocity at the inlet duct. From these measured values it was possible to determine the heat output of the collector and its thermal efficiency. The tests were performed for a range of irradiance  $G = 0\text{--}540\text{ W/m}^2$ . At maximum irradiance  $G_{\max} = 540\text{ W/m}^2$ , the measured value of temperature increase  $\Delta T = 38\text{ K}$ , air velocity at inlet  $w = 1.1\text{ m/s}$ , volumetric air flow rate  $V = 30\text{ m}^3/\text{h}$ , heat output  $Q = 386\text{ W}$  and thermal efficiency  $\eta = 36\%$ .

The obtained experimental results were compared with available research results wherever this was possible.

In relation to similar collector designs with conventional glass cover, the cellular polycarbonate covered prototype exhibits similar levels of thermal efficiency. The impact of glazing material was shown through the parameter  $F_R(\tau\alpha)$  from Eq. (3.4), and accounts for optical properties of the system. In the prototype design presented in this work it is approximately 20% lower than the values reported in the literature for glass covered collector [30]. The similarity of levels of thermal efficiency was mainly achieved due to a good thermal insulation of the prototype collector, presented by the parameter  $F_R U_L$  and the low slope of the efficiency characteristic in Fig. 10. The cellular polycarbonate material is a preferred choice when weight and safety issues (non-shattering material) are of importance.

## 5. FURTHER RESEARCH

Further research is needed to determine the impact of different absorber designs on passive solar air collector performance. An absorber with larger surface will improve heat transfer from the absorber to the air flowing through the collector. It is also desired to establish a clear conclusion on the impact of different glazing materials on thermal efficiency for passive solar air collectors that are driven by natural convection. New experimental cases are planned, and some of them include the collector being mounted on an exterior wall of a building, while other cases will concentrate on the influence of angle of inclination on incident radiation. It is likely that computational fluid dynamics (CFD) will be employed as an auxiliary tool to investigate various flow cases and prototype variants. Furthermore, this will allow for a comparison between numerical and experimental data.

## REFERENCES

1. LEWANDOWSKI W.M., *Pro-ecological, renewable energy sources* [in Polish], WNT, Warszawa 2007.
2. PN EN ISO 9488. *Solar Energy – Vocabulary*.
3. AFRIYIE J.K., NAZHA M.A.A., RAJAKARUNA H., FORSON F.K., *Experimental investigations of a chimney-dependent solar crop dryer*, *Renewable Energy*, **34**(1): 217–222, 2009.
4. FUDHOLI A., SOPIAN K., RUSLAN M.H., ALGHOUL M.A., SULAIMAN M.Y., *Review of solar dryers for agricultural and marine products*, *Renewable and Sustainable Energy Reviews*, **14**(1): 1–30, 2010.
5. YUSOFF W.F.M., SALLEH E., ADAM N.M., SAPIAN A., YUSOF S. M., *Enhancement of stack ventilation in hot and humid climate using a combination of roof solar collector and vertical stack*, *Building and Environment*, **45**(10): 2296–2308, 2010.
6. BOUADILA S., KOOLI S., LAZAAR M., SKOURI S., FARHAT A., *Performance of a new solar air heater with packed-bed latent storage energy for nocturnal use*, *Applied Energy*, **110**: 267–275, 2013.
7. GAN G., *Simulation of buoyancy-induced flow in open cavities for natural ventilation*, *Energy and Buildings*, **38**(5): 410–420, 2006.
8. MIYAZAKI T., AKISAWA A., KASHIWAGI T., *The effects of solar chimneys on thermal load mitigation of office buildings under the Japanese climate*, *Renewable Energy*, **31**(7): 987–1010, 2006.
9. NEMATOLLAHI O., ALAMDARI P., ASSARI M.R., *Experimental investigation of a dual purpose solar heating system*, *Energy Conversion and Management*, **78**: 359–366, 2014.
10. BENLI H., DURMUS A., *Performance analysis of a latent heat storage system with phase change material for new designed solar collectors in greenhouse heating*, *Solar Energy*, **83**(12): 2109–2119, 2009.
11. BENLI H., *Experimentally derived efficiency and exergy analysis of a new solar air heater having different surface shapes*, *Renewable Energy*, **50**: 58–67, 2013.
12. MANEewan S., KHEDARI J., ZEGHMATI B., HIRUNLABH J., EAKBURANAWAT J., *Experimental investigation on generated power of thermoelectric roof solar collector*, *Proceedings of 22nd International Conference on Thermoelectrics (ICT)*, pp. 574–577, 2003.
13. TOURE S., *Characteristic temperatures in a natural convection solar air heater*, *Energy Conversion and Management*, **42**(9): 1157–1168, 2001.
14. *Operation principles of passive air solar collectors* [in Polish, online]. URL: <http://flow-ex.pl/zasada-dzia-ania.html>.
15. ZHOU Y., JING G.E., LIU X.H., LI Q.L., *Research for ventilation properties of solar chimney with vertical collector*, *Procedia Environmental Sciences*, **11**(Part C): 1072–1077, 2011.
16. ARCE J., JIMÉNEZ M.J., GUZMÁN J.D., HERAS M.R., ALVAREZ G., XAMÁN J., *Experimental study for natural ventilation on a solar chimney*, *Renewable Energy*, **34**(12): 2928–2934, 2009.

17. CHEN Z.D., BANDOPADHAYAY P., HALLDORSSON J., BYRJALSEN C., HEISELBERG P., LI Y., *An experimental investigation of a solar chimney model with uniform wall heat flux*, Building and Environment, **38**(7): 893–906, 2003.
18. ALVAREZ G., ARCE J., LIRA L., HERAS L.M.R., *Thermal performance of an air solar collector with an absorber plate made of recyclable aluminium cans*, Solar Energy, **77**(1): 107–113, 2004.
19. OZGEN F., ESEN M., ESEN H., *Experimental investigation of thermal performance of a double-flow solar air heater having aluminium cans*, Renewable Energy, **34**(11): 2391–2398, 2009.
20. ESEN H., OZGEN F., ESEN M., SENGUR A., *Modelling of a new solar air heater through least-squares support vector machines*, Expert Systems with Applications, **36**(7): 10673–10682, 2009.
21. DUTKOWSKI K., PIĄTKOWSKI P., *Experimental investigation of a prototype passive solar air collector with polycarbonate cellular cover* [in Polish], Instal, **3**(360): 17–22, 2015.
22. TANAKA H., NAKATAKE Y., TANAKA M., *Indoor experiments of the vertical multiple-effect diffusion-type solar still coupled with a heat-pipe solar collector*, Desalination, **177**(1–3): 291–302, 2005.
23. BONCA Z., BUTRYMOWICZ D., HAJDUK T., TARGAŃSKI W., *New coolants and heat mediums. Thermal and performance properties* [in Polish], IPPU MASTA, Gdańsk 2004.
24. KARIM M.A., HAWLADER M.N.A., *Development of solar air collectors for drying applications*, Energy Conversion and Management, **45**(3): 329–344, 2004.
25. KARIM M.A., HAWLADER M.N.A., *Performance evaluation of a v-groove solar air collector for drying applications*, Applied Thermal Engineering, **26**(1): 121–130, 2006.
26. RYAN D., BUREK S.A.M., *Experimental study of the influence of collector height on the steady state performance of a passive solar air heater*, Solar Energy, **84**(9): 1676–1684, 2010.
27. ZHAI X.Q., DAI Y.J., WANG R.Z., *Experimental investigation on air heating and natural ventilation of a solar air collector*, Energy and Buildings, **37**(4): 373–381, 2005.
28. EL-SAWI A.M., WIFI A.S., YOUNAN M.Y., ELSAYED E.A., BASILY B.B., *Application of folded sheet metal in flat bed solar air collectors*, Applied Thermal Engineering, **30**(8–9): 864–871, 2010.
29. DUFFIE J.A., BECKMAN W.A., *Solar engineering of thermal processes*, 4th ed., Wiley, 2013.
30. PENG D., ZHANG X., DONG H., LV K., *Performance study of a novel solar air collector*, Applied Thermal Engineering, **30**(16): 2594–2601, 2010.
31. GILL R.S., SINGH S., SINGH P.P., *Low cost solar air heater*, Energy Conversion and Management, **57**: 131–142, 2012.
32. RAMANI B M., GUPTA A., KUMAR R., *Performance of a double pass solar air collector*, Solar Energy, **84**(11): 1929–1937, 2010.

Received February 24, 2016; accepted version June 30, 2016.

---